Available online at www.sciencedirect.com
ScienceDirect
Journal of Power Sources 178 (2008) 151–162
JOURNAL OF POWER SOURCES
www.elsevier.com/locate/jpowsour

Optimization of the interface polarization of the La_2NiO_4-based cathode working with the $Ce_{1-x}Sm_xO_{2-\delta}$ electrolyte system

D. Pérez-Coll [a,*], A. Aguadero [a], M.J. Escudero [a], P. Núñez [b], L. Daza [a,c]

[a] *Centro de Investigaciones Energéticas, Medioambientales y Tecnológicas (CIEMAT), Av. Complutense 22, 28040 Madrid, Spain*
[b] *Dpto. Química Inorgánica, Universidad de La Laguna, 38200 La Laguna, Tenerife, Spain*
[c] *Instituto de Catálisis y Petroleoquímica (CSIC), Marie-Curie 2, Campus Cantoblanco, 28049 Madrid, Spain*

Received 2 November 2007; received in revised form 5 December 2007; accepted 8 December 2007
Available online 1 February 2008

Abstract

The performance of La_2NiO_4 cathode material and $Ce_{1-x}Sm_xO_{2-\delta}$ ($x = 0.1, 0.2, 0.3, 0.4$) electrolyte system was analyzed. Ceria-based materials were prepared by the freeze-drying precursor route whereas La_2NiO_4 was prepared by the nitrate–citrate procedure. Electrolyte pellets were obtained after sintering the powders at 1600 °C for 10 h. Also dense ceria-based electrolytes samples were obtained by calcining the powders at 1150 °C after the addition of 2 mol%-Co. Interface polarization measurements were performed by impedance spectroscopy in air at open circuit voltage, using symmetrical cells prepared after the deposition of porous La_2NiO_4-electrodes on the $Ce_{1-x}Sm_xO_{2-\delta}$ system. X-ray diffraction (XRD) of cathode materials after using in symmetrical cells confirmed no significant reaction between La_2NiO_4 and ceria-based electrolytes. The efficiency of the cathode material is highly dependent on the composition of the electrolyte, and low-content Sm-doped ceria samples revealed an important decrease in the performance of the system. Differences in electrochemical behaviour were attributed principally to the oxide ion transference between cathode and electrolyte, and were correlated to the conductivity of the electrolyte. In this way cobalt-doped electrolytes with a Sm-content $\leq$30% perform better than free-cobalt samples due to the increase in grain boundary conductivity. Finally, composites of the ceria-based materials and La_2NiO_4 to use as cathode were prepared and an important increase of the interface performance was observed compared to La_2NiO_4 pure cathode. Predictions of maximun power density were obtained by the mixed transport properties of the electrolytes and by the interface polarization results. The use of composite materials could allow to increase the performance of the cell from 170 mW cm^{-2} for pure La_2NiO_4 cathode, to 370 mW cm^{-2} for La_2NiO_4–$Ce_{0.8}Sm_{0.2}O_{2-\delta}$ cathode, both working with $Ce_{0.8}Sm_{0.2}O_{2-\delta}$ electrolyte 300 μm in thickness and Ni–$Ce_{0.8}Sm_{0.2}O_{2-\delta}$ as anode at 800 °C.

Keywords: Solid oxide fuel cell; La_2NiO_4 cathode; Electrode polarization; Ceria electrolyte; Mixed conducting oxides

1. Introduction

Intermediate solid oxide fuel cells (IT-SOFC) have very important limitations due to the voltage drop in the internal components caused by the relatively high internal resistance at the operating temperatures (500–700 °C) [1]. The ohmic loss is mainly governed by the electrolyte resistance which is usually decreased by the reduction of the electrolyte thickness. On the other hand, the high cathode polarization is the main problem concerned to the interfacial resistances. The development of mixed ionic–electronic conducting materials is a promising way to decrease the polarization losses due to an enlargement of the electrochemical reaction zone [2,3]: from the triple-phase boundary (TPB) into a double contact between the gas phase and the mixed conductor. The family of compounds $A_2MO_{4+\delta}$ with the K_2NiF_4-type structure has been recently proposed due to the high electronic conductivity and some oxygen overstoichiometry which improves the oxygen ionic conduction by the high mobility of the interstitial lattice sites [4,5]. The overstoichiometric $La_2NiO_{4+\delta}$ has been reported to exhibit a metal (high T)-to-insulator (low T) transition as a function of temperature, displaying a maximum value of 82 S cm^{-1} at around 400 °C [6] and to present one of the highest oxygen diffusion values among different compounds with the K_2NiF_4-type structure [7]. Low

* Corresponding author. Tel.: +34 913 466 622; fax: +34 913 466 269.
E-mail address: domingo.perez@ciemat.es (D. Pérez-Coll).

0378-7753/$ – see front matter © 2007 Elsevier B.V. All rights reserved.
doi:10.1016/j.jpowsour.2007.12.030

values of electrode–electrolyte interface resistances are required in order to use these cathodes in SOFC. Commonly the analysis of this polarization process is performed paying more attention to the cathode properties than to the electrolyte ones. However, the optimization of the interfacial resistance needs the simultaneous knowledge of both cathode and electrolyte properties.

The present work analyzes the electrochemical performance of the La_2NiO_4-based cathode material with the $Ce_{1-x}Sm_xO_{2-\delta}$-based electrolyte system. The electrode polarization was studied by impedance spectroscopy in air, whereas the mixed transport properties of the electrolytes were analyzed by the Hebb–Wagner technique and impedance spectroscopy in air previously reported [8]. Important differences in the cathode performance were obtained by changing both the electrolyte and the electrode properties. The improvement of the electrolyte–grain boundary conduction seems to be an important feature for the optimization of the polarization process.

2. Experimental

2.1. Synthesis and structural characterization.

Freeze-drying precursor route [9,10] was used to prepare $Ce_{1-x}Sm_xO_{2-\delta}$ ($x = 0.1$, 0.2, 0.3, 0.4) powders. Stoichiometric amounts of cations were dissolved in distilled water using the following nitrates as reactants: $Ce(NO_3)_3{\cdot}6H_2O$ (Aldrich, 99.99%), $Sm(NO_3)_3{\cdot}6H_2O$ (Aldrich, 99.9%). The solutions were frozen in liquid nitrogen and introduced in a freeze-dryer (Heto Lyolab) for 3 days. The amorphous powders were then calcined at 375 °C for 4 h to decompose the nitrates. X-ray diffraction measurements (Philips X'Pert powder diffractometer; Cu Kα radiation, $\lambda = 1.5406$ Å) were performed to analyze the crystal structure of the powders calcined at low and high temperatures. Lattice parameters were extracted from X-ray diffraction (XRD) patterns from powders calcined at 1600 °C for 10 h.

Sintered pellets of about 7-mm diameter and 1-mm thickness were prepared by uniaxial pressing after milling the powders (precalcined at 375 °C) with zirconia balls and calcining at 1600 °C for 10 h.

The use of 2 mol% of cobalt as sintering additive allowed the decrease of sintering temperature [8,11,12], and high-density pellets were obtained calcining at 1150 °C for 10 h. Cobalt was previously added by impregnating the precalcined powders with an ethanol solution of $Co(NO_3)_2{\cdot}6H_2O$ (Panreac, purity > 98%) and heating at 650 °C for 1 h.

Polycrystalline $La_2NiO_{4+\delta}$ powder was synthesized via a nitrate–citrate route. Stoichiometric amounts of analytical grade of La_2O_3 and $Ni(NO_3)_2{\cdot}6H_2O$ (Panreac) were dissolved in citric acid (10%) with some drops of HNO_3 (65%) under stirring. The solution was slowly evaporated, leading to an organic resin which was dried at 120 °C and slowly decomposed at temperatures up to 600 °C. Finally, it was fired in air at 950 °C for 8 h and slowly cooled down to room temperature. The prepared samples were characterized by XRD for phase identification and to assess phase purity.

2.2. Preparation of the cell and microstructural characterization

The electrochemical measurements of the cathode//electrolyte systems were performed on symmetrical cells. For this purpose, a slurry of the cathode material and a binder (Decoflux™, WB41, Zschimmer and Schwartz) was prepared, and the milled ink was symmetrically painted onto the surface of the sintered pellets obtaining 5.50 mm diameter symmetrical electrodes. The cell was then calcined at 1000 °C for 4 h to obtain a good adherence between the components. Symmetrical Pt electrodes were then painted over the cathode surface to ensure equipotential conditions and the cell was calcined at 950 °C for 30 min. As electrolytes, pellets obtained from the system $Ce_{1-x}Sm_xO_{2-\delta}$ ($x = 0.1$, 0.2, 0.3, 0.4) sintered at 1600 °C, and $Ce_{1-x}Sm_xO_{2-\delta}$ + 2%Co ($x = 0.1$, 0.2, 0.3, 0.4) sintered at 1150 °C were employed. In a first analysis powders of La_2NiO_4 as cathode were used. Then composites of La_2NiO_4–$Ce_{1-x}Sm_xO_{2-\delta}$ ($x = 0.1$, 0.2, 0.3, 0.4) in a ratio of 2:1 (w/w), respectively, were also prepared. Table 1 shows the symmetrical cell systems studied in the present work and the notation used for the sake of clarity.

In order to analyze the chemical compatibility of cathodes and electrolytes, XRD measurements were performed in cathode materials after being applied with the binder over the electrolyte pellets and calcined in the cell at 1000 °C for 4 h.

The thermal compatibility of $Ce_{1-x}Sm_xO_{2-\delta}$ system and La_2NiO_4 cathode material was studied by the thermal expansion of dense ceramics in air, using a Linseis L75/1550C dilatometer between 25 and 1000 °C, with a heating rate of 5 °C min^{-1}.

Scanning electron microscopy (Hitachi S-2500) measurements were performed on fracture and superficial surfaces of the studied cells to analyze the microstructure and possible reaction of the components.

2.3. Electrode performance characterization

The electrode activity of the La_2NiO_4-based material over the $Ce_{1-x}Sm_xO_{2-\delta}$ electrolyte system was evaluated by the interfacial polarization resistance in symmetrical cell configuration, and it was studied by impedance spectroscopy in air at open circuit voltage (AUTOLAB PGSTAT 302, ECO CHEMIE). Experimental measurements were performed by decreasing the temperature from 1000 to 500 °C, in the frequency range of 10^{-2} to 10^6 Hz and an excitation voltage of 50 mV. Zview 2.9c software (Scribner Associates) was used to fit the experimental data to the equivalent circuits. The polarization data were multiplied by the electrode area and 0.5 to account for both electrodes.

2.4. Mixed conducting properties of ceria–samaria-based electrolytes

Ionic transport properties of the system $Ce_{1-x}Sm_xO_{2-\delta}$ ($x = 0.05$, 0.1, 0.2, 0.3) were previously reported for pellets sintered at 1600 °C [8] and a high influence of the Sm-content was observed. High-temperature sintered samples showed resistive grain boundaries, more valuable in Sm-low content pellets

Table 1
Symmetrical cells and components studied in this work

Symmetrical cell: electrode//electrolyte	Cathode material	Electrolyte
La_2NiO_4//10CSO	La_2NiO_4	$Ce_{0.9}Sm_{0.1}O_{2-\delta}$
La_2NiO_4//20CSO	La_2NiO_4	$Ce_{0.8}Sm_{0.2}O_{2-\delta}$
La_2NiO_4//30CSO	La_2NiO_4	$Ce_{0.7}Sm_{0.3}O_{2-\delta}$
La_2NiO_4//40CSO	La_2NiO_4	$Ce_{0.6}Sm_{0.4}O_{2-\delta}$
La_2NiO_4//10CSO2Co	La_2NiO_4	$Ce_{0.9}Sm_{0.1}O_{2-\delta}$ + 2%Co
La_2NiO_4//20CSO2Co	La_2NiO_4	$Ce_{0.8}Sm_{0.2}O_{2-\delta}$ + 2%Co
La_2NiO_4//30CSO2Co	La_2NiO_4	$Ce_{0.7}Sm_{0.3}O_{2-\delta}$ + 2%Co
La_2NiO_4//40CSO2Co	La_2NiO_4	$Ce_{0.6}Sm_{0.4}O_{2-\delta}$ + 2%Co
La_2NiO_4–10CSO//20CSO	La_2NiO_4–$Ce_{0.9}Sm_{0.1}O_{2-\delta}$ (2:1 (w/w))	$Ce_{0.8}Sm_{0.2}O_{2-\delta}$
La_2NiO_4–20CSO//20CSO	La_2NiO_4–$Ce_{0.8}Sm_{0.2}O_{2-\delta}$ (2:1 (w/w))	$Ce_{0.8}Sm_{0.2}O_{2-\delta}$
La_2NiO_4–30CSO//20CSO	La_2NiO_4–$Ce_{0.7}Sm_{0.3}O_{2-\delta}$ (2:1 (w/w))	$Ce_{0.8}Sm_{0.2}O_{2-\delta}$
La_2NiO_4–40CSO//20CSO	La_2NiO_4–$Ce_{0.6}Sm_{0.4}O_{2-\delta}$ (2:1 (w/w))	$Ce_{0.8}Sm_{0.2}O_{2-\delta}$
La_2NiO_4–20CSO//20CSO2Co	La_2NiO_4–$Ce_{0.8}Sm_{0.2}O_{2-\delta}$ (2:1 (w/w))	$Ce_{0.8}Sm_{0.2}O_{2-\delta}$ + 2%Co

Note that in impedance spectroscopy measurements the cathode materials were placed in symmetrical configuration, that is on both surfaces of the electrolytes

($x = 0.05$, 0.1). However, the addition of cobalt and sintering at 1150 °C decreased the grain boundary resistivity. The space charge layer model was proposed to account modifications in Sm and/or Co segregation at grain boundaries.

The use of ceria-based systems in fuel-cell conditions, makes necessary the analysis of electronic conductivity under reducing conditions. For this purpose Hebb–Wagner/ion-blocking measurements [13–16] in $Ce_{1-x}Sm_xO_{2-\delta}$ ($x = 0.1$, 0.2, 0.3) pellets sintered at 1600 °C (cobalt-free samples) and 1150 °C (cobalt-doped samples) were performed. Table 2 shows the notation used for the electrolytes. High-dense pellets were sealed against an alumina impervious disk obtaining an ion-blocking electrode after applying the inner under cathodic polarization. Reference electrode was in air conditions and the oxygen partial pressure in the blocking electrode was decreased by the increase in the cathodic polarization. More details of the experimental setup were presented elsewhere [10,17]. The electronic conductivity under the chemical potential gradient was extracted by the average electronic conductivity for the conditions across the sample, as follows:

$$\sigma_{e,av} = \frac{L}{A}\frac{I_e}{V_0} \quad (1)$$

where L and A are the sample thickness and the electrode area respectively; V_0 is the steady-state potential difference across the sample and I_e is the steady-state electronic current.

Table 2
Sintering temperature, unit cell parameter and densification of the electrolytes

Electrolyte	Notation	T_s (°C)	a (Å)	Densification (%)
$Ce_{0.9}Sm_{0.1}O_{2-\delta}$	10CSO	1600	5.4236(2)	98
$Ce_{0.8}Sm_{0.2}O_{2-\delta}$	20CSO	1600	5.4351(1)	99
$Ce_{0.7}Sm_{0.3}O_{2-\delta}$	30CSO	1600	5.4447(1)	96
$Ce_{0.6}Sm_{0.4}O_{2-\delta}$	40CSO	1600	5.4508(2)	99
$Ce_{0.9}Sm_{0.1}O_{2-\delta}$ + 2%Co	10CSO2Co	1150	5.4233(2)	97
$Ce_{0.8}Sm_{0.2}O_{2-\delta}$ + 2%Co	20CSO2Co	1150	5.4347(2)	97
$Ce_{0.7}Sm_{0.3}O_{2-\delta}$ + 2%Co	30CSO2Co	1150	5.4443(2)	95
$Ce_{0.6}Sm_{0.4}O_{2-\delta}$ + 2%Co	40CSO2Co	1150	5.4506(1)	98

3. Results

3.1. Synthesis, characterization and compatibility of electrolytes and cathode materials

Powders of $Ce_{1-x}Sm_xO_{2-\delta}$ ($x = 0.1$, 0.2, 0.3, 0.4) calcined at 375 °C for 4 h presented flourite single phases as it was confirmed by XRD measurements. Lattice parameters were extracted from XRD patterns from powders calcined at 1600 °C for 10 h and it was observed a linear increase with Sm addition, for x increasing from 0.1 to 0.3 (Table 2). Sample doped with $x = 0.4$ deviates from linearity due to the approximation to the doping-saturation limit, as it was also found in Gd-doped system [18].

XRD measurements were also performed in cobalt-doped ceria–samaria powders calcined at 1150 °C for 10 h, and it was confirmed no evidences of secondary phases and no significant changes in lattice parameters compared to cobalt-free samples (Table 2). Cobalt-free pellets sintered at 1600 °C and cobalt-doped pellets sintered at 1150 °C presented high values of densification (≥95%) as it is also shown in Table 2.

$La_2NiO_{4+\delta}$ powders calcined at 950 °C for 8 h possessed the pure and well-crystallized K_2NiF_4 structure, as it was also confirmed by XRD data.

The chemical stability between the electrode and electrolytes was also analyzed by means of X-ray diffraction. There is no significant reaction between $La_2NiO_{4+\delta}$ and $Ce_{1-x}Sm_xO_{2-\delta}$ ($x = 0.1$, 0.2, 0.3, 0.4) when the cathode is placed on the electrolyte and calcined at 1000 °C for 4 h, as it is appreciable in Fig. 1(a) and (b) for La_2NiO_4//20CSO. However, there is a slight reaction between $La_2NiO_{4+\delta}$ and $Ce_{1-x}Sm_xO_{2-\delta}$ ($x = 0.1$, 0.2, 0.3, 0.4) in the composites $La_2NiO_{4+\delta}$–$Ce_{1-x}Sm_xO_{2-\delta}$ (2:1 (w:w)) when they are previously mixed, placed on the electrolytes and heated at 1000 °C during 4 h, leading to the

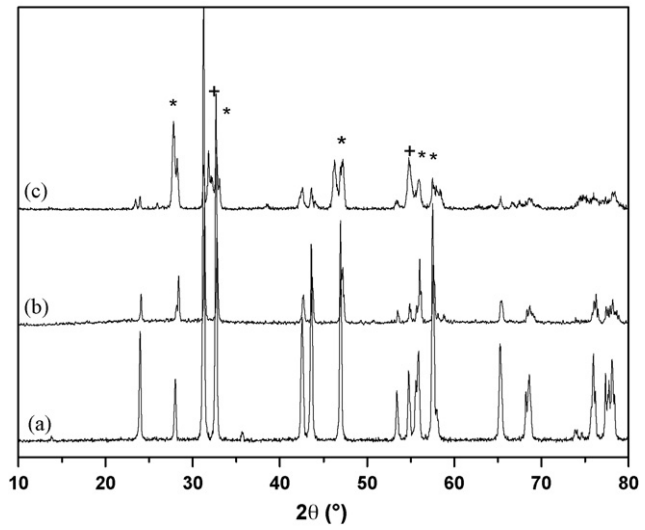

Fig. 1. X-ray diffraction patterns for (a) pure well-crystallized La_2NiO_4 phase; (b) La_2NiO_4 placed on 20CSO electrolyte and calcined at 1000 °C for 4 h; (c) composite La_2NiO_4–20CSO (2:1 (w:w)) deposited on 20CSO electrolyte and calcined at 1000 °C for 4 h. Note that (*) indicates most important peaks of 20CSO and (+) most important peaks of $La_3Ni_2O_7$.

formation of the Ruddlesden–Popper $La_3Ni_2O_7$ as a secondary phase (Fig. 1(c)). Similar behaviour was observed in cobalt-doped electrolytes.

Aiming to study the mechanical compatibility of the $La_2NiO_{4+\delta}$ electrode with the $Ce_{1-x}Sm_xO_{2-\delta}$ electrolytes, thermal expansion measurements of dense ceramics were carried out in air. Fig. 2 illustrates the $\Delta L/L_0$ values obtained using a heating rate of 5 °C min^{-1} in the range of 30–1000 °C. The calculated thermal expansion coefficients (TEC) are in the range of 11.4–12.6 × 10^{-6} K^{-1}, for $Ce_{1-x}Sm_xO_{2-\delta}$ electrolytes, which match well with the obtained 12.4 × 10^{-6} K^{-1} value for $La_2NiO_{4+\delta}$.

Fig. 3(a) shows a cross-section SEM image of a porous $La_2NiO_{4+\delta}$ electrode deposited on a dense 20CSO2Co electrolyte. It is observed a good adherence between the electrolyte

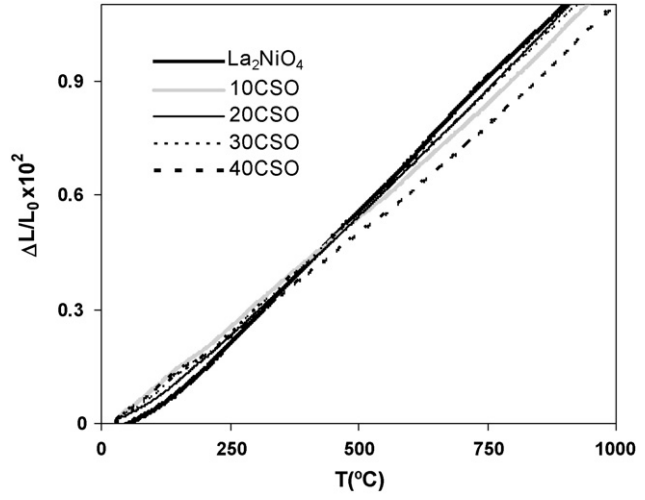

Fig. 2. Thermal expansion measurements for La_2NiO_4 and $Ce_{1-x}Sm_xO_{2-\delta}$ series with $x = 0.1$, 0.2, 0.3 and 0.4.

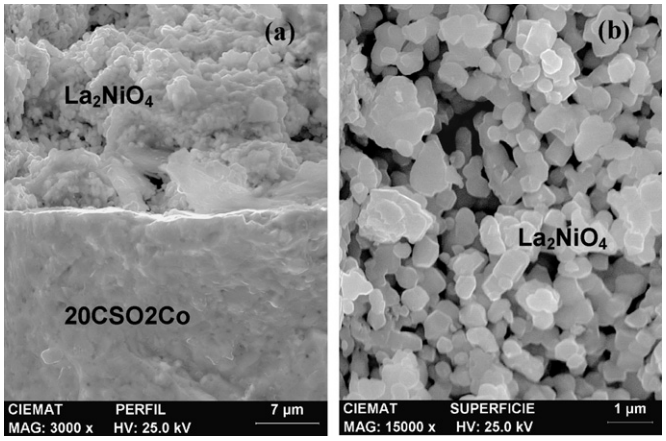

Fig. 3. SEM images of the La_2NiO_4//20CSO2Co cell. (a) Cross-section image of the electrolyte and the cathode and (b) superficial image of the porous cathode.

and the cathode layer with neither cracks nor discontinuity points along the cathode–electrolyte interface. Also it is evidenced the high densification of the electrolyte (≥95%) and the porosity of the cathode layer (Fig. 3(b)).

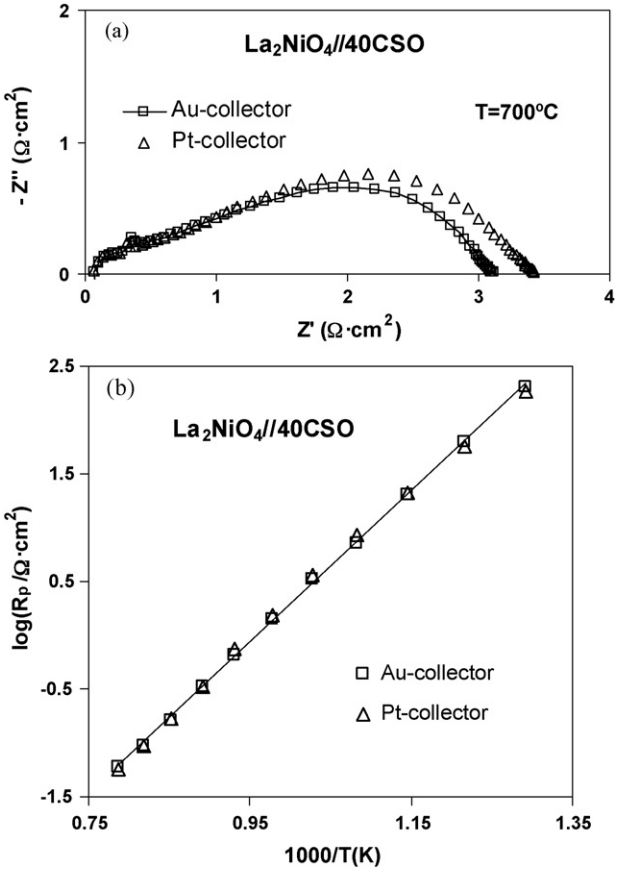

Fig. 4. Impedance spectra obtained at 700 °C (a), and area-specific resistance of the polarization process in the entire range of temperature (b), for the symmetrical cell configuration La_2NiO_4//40CSO with current collectors based on Au-ink (squares) and Pt-ink (triangles).

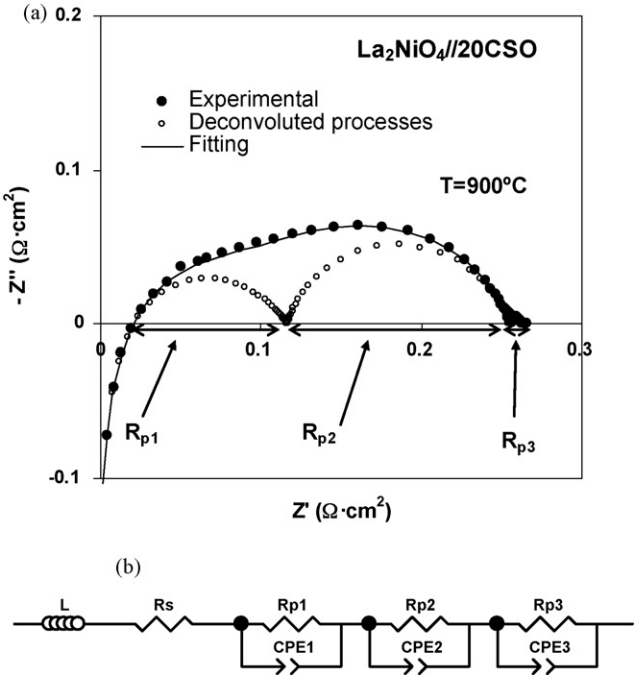

Fig. 5. (a) Impedance spectroscopy data for La_2NiO_4//20CSO system measured at 900 °C (closed circles). Electrolyte resistance (R_s) was subtracted from the experimental data. Also it is shown the fitting data (line) and each deconvoluted polarization process (open circles). (b) Equivalent circuit used for fitting the experimental data.

3.2. La_2NiO_4 cathode material with $Ce_{1-x}Sm_xO_{2-\delta}$ electrolyte system

The application of the equipotential conditions to the electrode surfaces during impedance spectroscopy measurements was ensured by the use of porous Pt over the cathode material as current collector. To confirm the absence of an extra-catalytic effect associated to the Pt current collector, two configurations of the symmetrical cell La_2NiO_4//40CSO were prepared: first with porous Pt as current collector, and after that with porous Au electrodes. Fig. 4(a) shows the impedance spectra obtained in both cases at 700 °C and it is clearly observed that the total polarization resistance of the interface is practically not affected by the current collector employed. This suggests that the porous Pt does not introduce an extra-catalytic effect in the interface polarization process, as it is confirmed by the representation of the area-specific resistance in the entire range of the studied temperature (Fig. 4(b)).

Electrode polarization processes of the studied systems are characterized by three different contributions as it is shown in Fig. 5(a) for La_2NiO_4//20CSO symmetrical cell, in which each polarization contribution was adjusted to a R_p-CPE element (Fig. 5(b)). Note that in the spectra is also appreciable at high frequencies the induction process coming from the measurement setup. The represented spectra were displaced to the origin of the x-axis after the subtraction of the series resistances. This allows an easier comparison of the polarization processes. To take into account these two contributions in the fitting of the experimental data the elements L and R_s were introduced, respectively. The high frequency arc is usually attributed to the oxygen ion transference from the electrode–electrolyte interface into the electrolyte [19,20]. This process may be governed by the ionic transport of the electrolyte and should not be dependent on the oxygen partial pressure [21]. The intermediate frequency arc could be attributed to the charge transfer reaction, and the low frequency arc to the oxygen diffusion process [22]. Fig. 6(a) shows an example of the impedance spectra obtained at 900 °C for the La_2NiO_4 cathode placed in symmetrical configuration onto the electrolytes 10CSO, 20CSO, 30CSO and 40CSO. Clear differences were obtained for the electrolytes employed: total interface polarization resistance decreases when the Sm-content increases, in the entire range of temperature (Fig. 6(b)). The high electrode polarization resistance of 1.64 Ω cm^2 at 800 °C when using 10CSO electrolyte is decreased to 1.00, 0.77 and 0.73 Ω cm^2 when the electrolytes are 20CSO, 30CSO and 40CSO, respectively. It was previously reported systematic studies of the ionic conductivity of ceria-based electrolytes doped with different contents of Gd and Sm [8,18]. These results clearly indicated that samples sintered at 1600 °C presented a monotonous decrease of the grain boundary resistivity when the

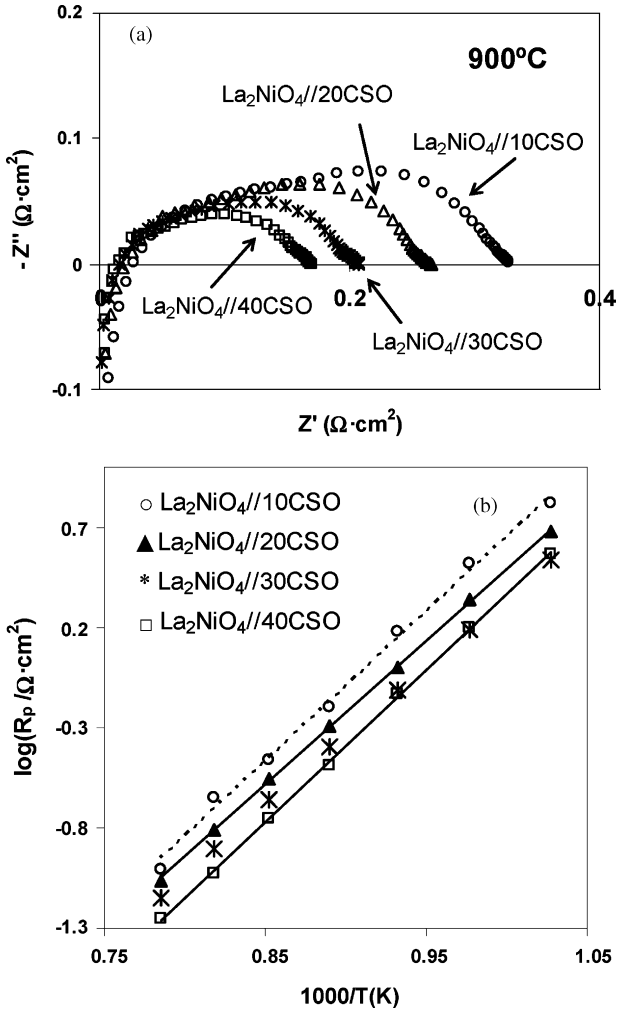

Fig. 6. (a) Impedance spectra at 900 °C for La_2NiO_4 cathode material over $Ce_{1-}Sm_xO_{2-\delta}$ (x = 0.1, 0.2, 0.3, 0.4) electrolytes sintered at 1600 °C and (b) area-specific resistances in the entire range of studied temperatures.

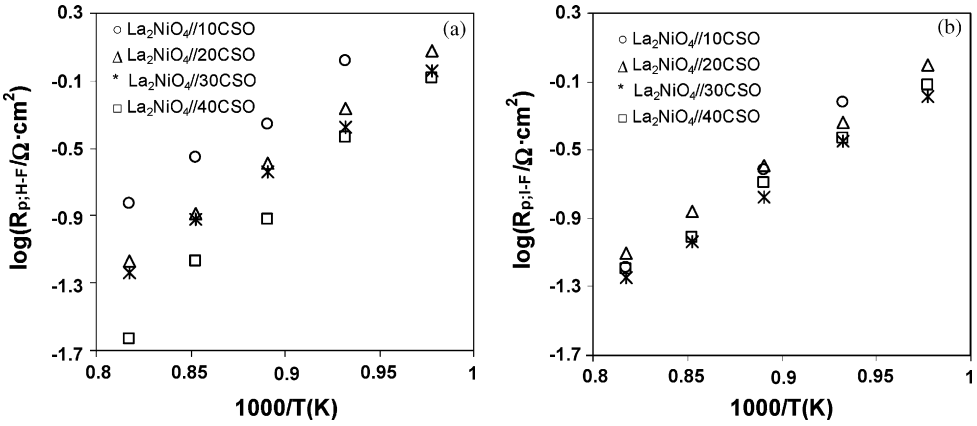

Fig. 7. (a) High-frequency polarization resistance for different Sm-content electrolytes with La_2NiO_4 cathode material and (b) intermediate-frequency polarization resistance.

Sm and/or Gd content increased. This was attributed to lower effects of the space charge potential, due to lower differences in composition between bulk and space charge layer. These results suggest that the grain boundary process could be determinant in the detriment of the electrode polarization process as it was also previously suggested for the system LSM–YSZ [21,23]. In this way Fig. 7(a) shows that the area-specific resistance of the high frequency polarization process increases when the Sm-content decreases, in good agreement with the increase in the grain boundary resistivity [8]. However, Fig. 7(b) shows that the intermediate-frequency polarization process, which is attributed to the charge transfer reaction, is not strongly affected by the Sm-content of the electrolyte, suggesting that total polarization is governed by the oxide ions transference from the interface cathode–electrolyte to the electrolyte. It is also to stand out that it has been studied the p-type electronic conductivity of $Ce_{1-x}Gd_xO_{2-\delta}$ and it was obtained an increase when the Gd-content increases [24], and as a consequence the oxygen surface exchange rate of the electrolyte increases. This phenomenon could also contribute to the enhancement of the electrochemical activity of samples doped with higher contents of Sm. It was previously reported the Pt-electrode polarization of the $Ce_{0.80}Gd_{0.20}O_{2-\delta}$ and $Ce_{0.80}Gd_{0.18}Pr_{0.02}O_{2-\delta}$ electrolytes and it was confirmed a decrease in the polarization resistance of

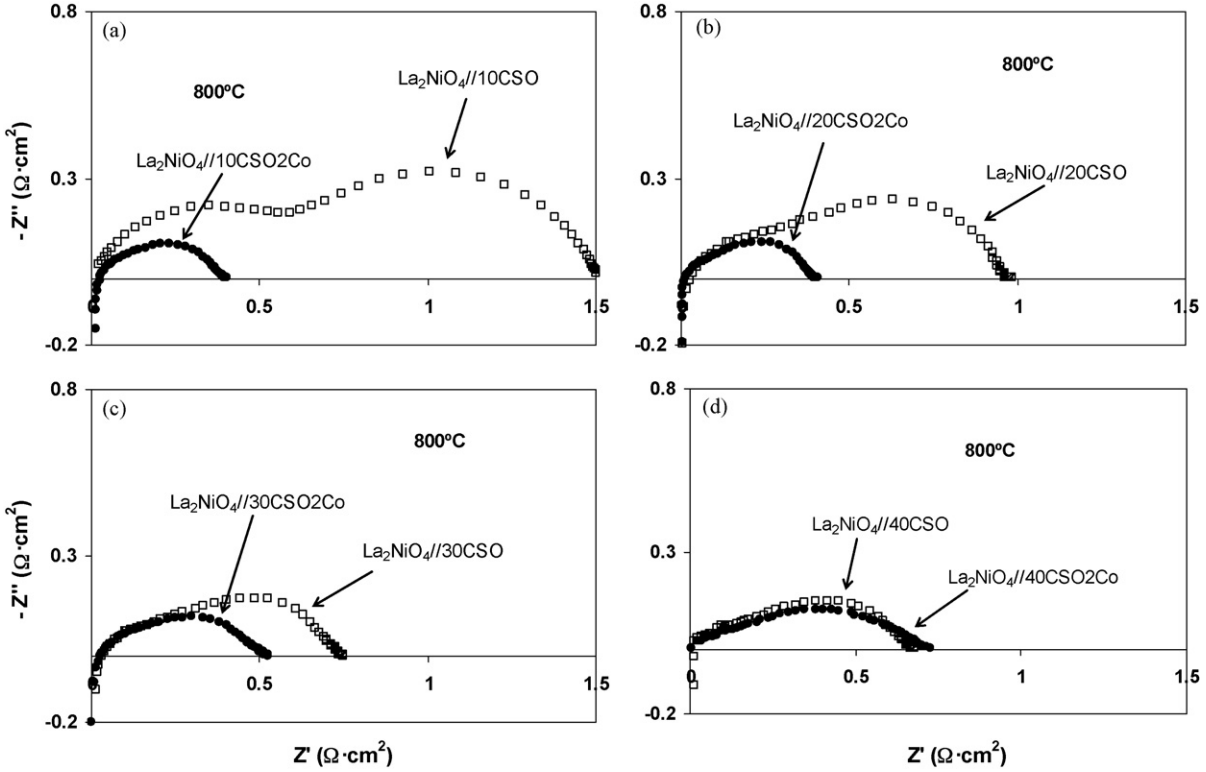

Fig. 8. Impedance spectra at 800 °C for La_2NiO_4-cathode material placed in symmetrical configuration over $Ce_{1-x}Sm_xO_{2-\delta}$ electrolytes with (closed symbols) and without (open symbols) cobalt addition. (a) $x = 0.1$; (b) $x = 0.2$; (c) $x = 0.3$; (d) $x = 0.4$.

Pr-doped samples [25]. However, the authors confirmed that the increase in the p-type electronic conductivity at the electrolyte surface was not the only factor to enhance the electrode activity.

3.3. La_2NiO_4 cathode material with $Ce_{1-x}Sm_xO_{2-\delta}$ + 2%Co electrolyte system

The ionic transport properties of the studied electrolyte system are highly influenced by the grain boundary. Important enhancement of the properties was reported by the addition of small amounts of cobalt and sintering at low temperature, mainly in samples with highly resistive grain boundaries [8,26]. The analysis of the performance of La_2NiO_4 electrode was extended to $Ce_{1-x}Sm_xO_{2-\delta}$ + 2%Co (T_s = 1150 °C) electrolyte system in order to account the effect of the enhanced grain boundary in the polarization resistance. Fig. 8 shows examples of the impedance spectra obtained for samples with and without cobalt as sintering additive. The polarization resistance clearly decreases in cobalt-added electrolytes (except for 40%Sm), and the effect is more pronounced in samples with low content of Sm (10%Sm, 20%Sm). Fig. 9 shows the analysis extended to the entire range of temperature. The enhancement in the performance of the electrode//electrolyte interface polarization produces a decrease in the resistance from 1.64 Ω cm^2 at 800 °C for 10CSO electrolyte to 0.40 Ω cm^2 for 10CSO2Co electrolyte. These results agree well with the previously reported behaviour of the grain boundary [8,18] in which the segregation of cobalt and sintering at low temperature could contribute to mitigate the deleterious effect associated to the segregation of impurities and/or Sm^{3+} at grain boundaries. This is observed in Fig. 10 for the comparison of La_2NiO_4//$Ce_{1-x}Sm_xO_{2-\delta}$-interface polarization resistance and electrolyte–grain boundary resistivity as a function of Sm-content in $Ce_{1-x}Sm_xO_{2-\delta}$ (T_s = 1600 °C) and $Ce_{1-x}Sm_xO_{2-\delta}$ + 2%Co (T_s = 1150 °C) electrolytes. It was also reported [8,18] that the classical Mott–Schottky space charge potential was clearly more affected by the addition of cobalt in highly resistive grain boundary samples that is in samples with lower contents of Sm^{3+}/Gd^{3+}. Now the results confirm the important role of the electrolyte grain boundary conduction in the polarization behaviour of the cathode–electrolyte interface. Note that the addition of cobalt was also reported to increase the p-type electronic conductivity in Gd-doped ceria [12,24], which could also increase, at least partially, the polarization activity of the electrode–electrolyte interface.

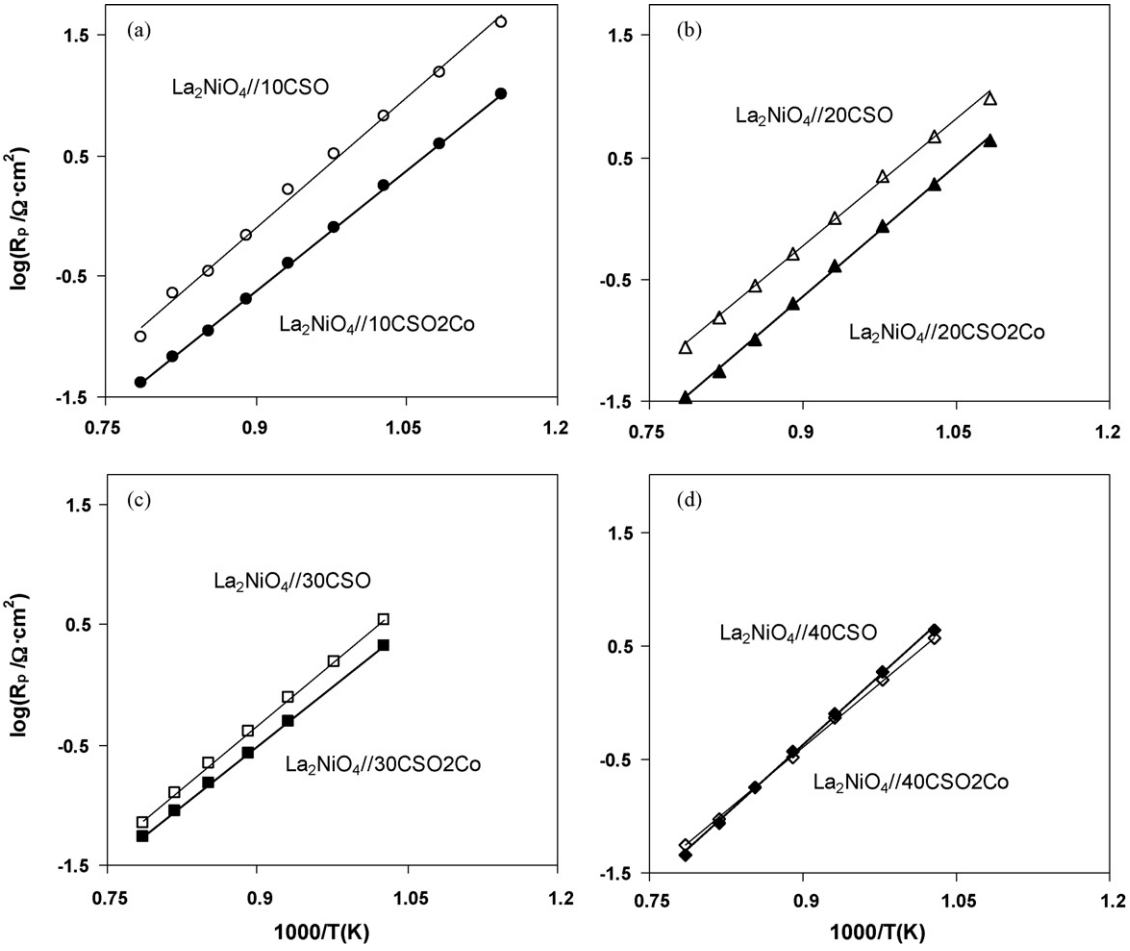

Fig. 9. Electrode polarization resistances for La_2NiO_4-cathode material over $Ce_{1-x}Sm_xO_{2-\delta}$ electrolytes with x = 0.1 (a); x = 0.2 (b); x = 0.3 (c); x = 0.4 (d), with cobalt-addition (closed symbols) and without cobalt addition (open symbols).

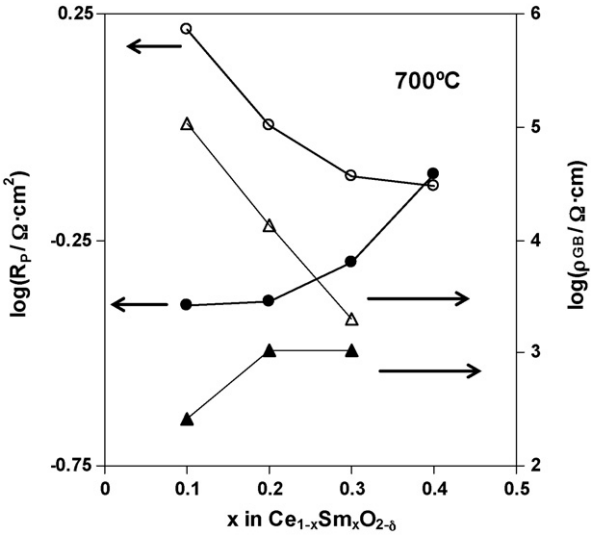

Fig. 10. Interface electrode/electrolyte polarization for La_2NiO_4//$Ce_{1-x}Sm_xO_{2-\delta}$ (circles) and electrolyte–grain boundary resistivity (triangles) as a function of Sm-content in the electrolyte. Closed symbols correspond to $Ce_{1-x}Sm_xO_{2-\delta}$ + 2%Co electrolytes.

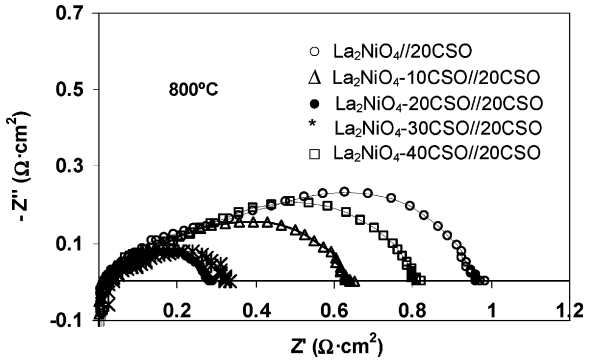

Fig. 11. Impedance spectra for La_2NiO_4–$Ce_{1-x}Sm_xO_{2-\delta}$ composites (2:1 (w:w)) placed over $Ce_{0.8}Sm_{0.2}O_{1.9}$ electrolyte in symmetrical configuration. Pure La_2NiO_4-cathode material is also shown for comparison.

3.4. Composites of La_2NiO_4-$Ce_{1-x}Sm_xO_{2-\delta}$ cathode materials with $Ce_{0.8}Sm_{0.2}O_{1.9}$ electrolyte

The catalytic activity of the electrode material was modified by the use of La_2NiO_4–$Ce_{1-x}Sm_xO_{2-\delta}$ composites, due to the introduction of the ionic conductor component extends the effective places of reaction. Powders of composites were prepared in a ratio of 2:1 (w/w) for La_2NiO_4 and $Ce_{1-x}Sm_xO_{2-\delta}$ respectively, and for $x = 0.1$, 0.2, 0.3, 0.4. The analysis was performed by the use of these electrode materials in symmetrical configuration placed on the $Ce_{0.8}Sm_{0.2}O_{1.9}$ electrolyte sintered at 1600 °C. Fig. 11 shows the impedance spectra in air obtained at 800 °C for the studied composites compared to the pure La_2NiO_4 cathode material. The use of composites produces an important decrease in the electrode polarization due to the increase of the mixed conducting properties of the cathode material. However, the increase in the electrode performance is not correlated to the increase in the Sm-content in $Ce_{1-x}Sm_xO_{2-\delta}$ system. Fig. 12(a) shows that the electrode polarization resistance presents a minimum for the composite La_2NiO_4–20CSO used as symmetrical electrode with the electrolyte 20CSO. On the other hand Fig. 12(b) shows the bulk ionic resistivity of the system $Ce_{1-x}Sm_xO_{2-\delta}$ extracted from results of Ref. [8] which also presents a minimum in $x = 0.2$. However, the effect produced by changes in composition of Sm-doped powders on the electrode polarization do not correspond to the bulk conductivity behaviour. This suggests that the ionic conductivity of the composite is not the only factor that affects the performance of the electrode, and different catalytic properties could be attributed to different Sm-content composites. Note that electrochemical properties of the interfaces formed by La_2NiO_4 and $Ce_{1-x}Sm_xO_{2-\delta}$ composite materials may be dependent on the Sm-content, affecting the performance of the system. Composite system of La_2NiO_4–20CSO presents very good properties to use as cathode material on 20CSO electrolyte with electrode polarization values of 0.29 and 0.76 Ω cm^2 at 800 and 750 °C, respectively. However, the efficiency of the system when used in a SOFC is also dependent on the electrolyte resistance, due to a decrease of the cell voltage (E) when current (I)

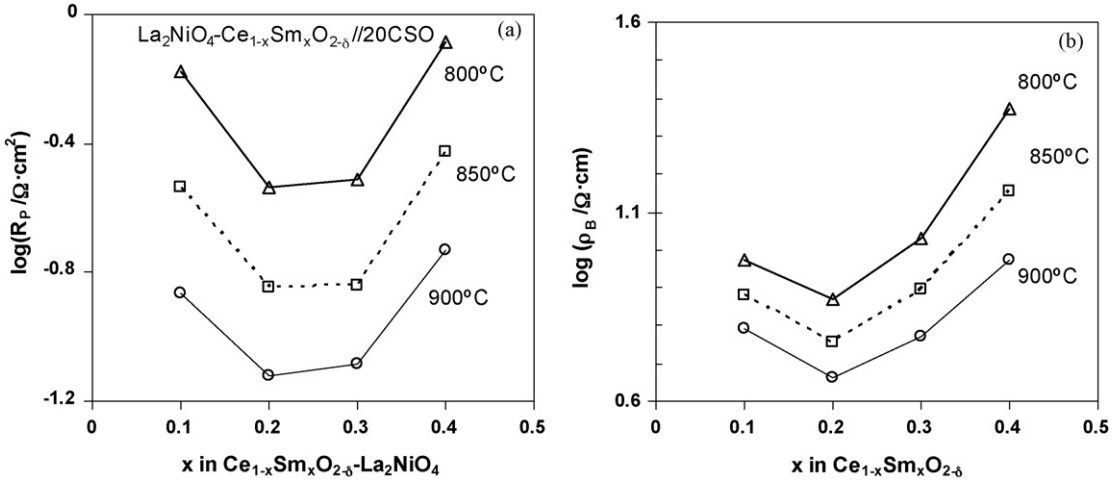

Fig. 12. (a) Electrode polarization resistance as a function of Sm-content in La_2NiO_4–$Ce_{1-x}Sm_xO_{2-\delta}$ composites placed in symmetrical configuration over $Ce_{0.8}Sm_{0.2}O_{1.9}$ electrolyte and (b) bulk ionic resistivity of $Ce_{1-x}Sm_xO_{2-\delta}$ system as a function of Sm-content.

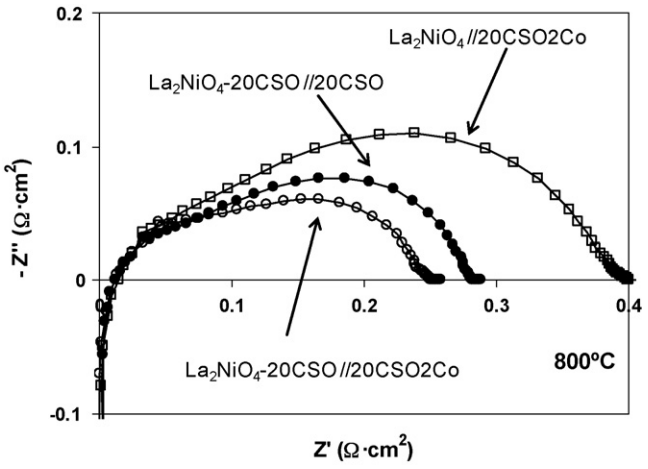

Fig. 13. Impedance spectra at 800 °C for composite La_2NiO_4–20CSO placed on the 20CSO electrolyte and 20CSO2Co electrolyte. For comparison it is also represented the spectra obtained for La_2NiO_4 over 20CSO2Co electrolyte.

is flowing, according to the following equation:

$$E = \mathrm{OCV} - IR_s - IR_{p,\mathrm{cath}} - IR_{p,\mathrm{anod}} \quad (2)$$

where OCV (open circuit voltage) is the voltage in the cell when current is zero; R_s is the total ohmic resistance of the cell, which is principally affected by the ionic resistance of the electrolyte; and $R_{p,\mathrm{cath}}$ and $R_{p,\mathrm{anod}}$ correspond to the interface polarization of the cathode and the anode with the electrolyte, respectively.

20CSO electrolyte sintered at very high temperature (1600 °C) is affected by resistive grain boundaries [8], even at intermediate temperatures, and it could decrease the efficiency of the system due to the increase in total resistance R_s (Eq. (2)). However, as it was mentioned, this problem is avoided by the addition of small amounts of cobalt as sintering additive and calcining at low temperature. The analysis was then extended to the use of 20CSO2Co (T_s = 1150 °C) as electrolyte, and the performance with La_2NiO_4–20CSO cathode composite was studied. Fig. 13 shows an example of the polarization resistance at 800 °C for the systems La_2NiO_4–20CSO//20CSO, La_2NiO_4–20CSO//20CSO2Co and La_2NiO_4//20CSO2Co. The use of 20CSO2Co as electrolyte was previously confirmed to increase the performance with La_2NiO_4 compared to the cobalt-free 20CSO electrolyte (Figs. 8 and 9). Now Fig. 13 reveals a very similar performance for 20CSO2Co electrolyte (0.26 Ω cm^2 at 800 °C) compared to 20CSO electrolyte (0.29 Ω cm^2) when used with the composite cathode-material La_2NiO_4–20CSO. In both cases the performance is better than those of the pure La_2NiO_4 with 20CSO2Co (0.41 Ω cm^2) and 20CSO (1.00 Ω cm^2) electrolytes. The results of ionic electrolyte conductivity, previously reported, and electrode polarization resistance suggest the use of 20CSO2Co electrolyte combined with the composite cathode La_2NiO_4–20CSO as the optimized semi-cell for SOFC applications.

3.5. Possible application in SOFC conditions

The use of the studied systems as cathode–electrolyte components of a SOFC is subordinated to the obtainment of high efficiencies, that is high values of power density, which is given by the following equation:

$$P = IE = I\mathrm{OCV} - I^2R_s - I^2R_{p,\mathrm{cath}} - I^2R_{p,\mathrm{anod}} \quad (3)$$

Using Eq. (3) it is easy to obtain the maximum power density, indicated by the following equation:

$$P_{\max} = \frac{\mathrm{OCV}^2}{4(R_s + R_{p,\mathrm{cath}} + R_{p,\mathrm{anod}})} \quad (4)$$

Eq. (4) indicates that the maximum efficiency of the system is not only dependent on the ionic resistance of the electrolyte and the cathode and anode polarization, but is also dependent on the OCV. The corresponding value of OCV for a mixed conducting

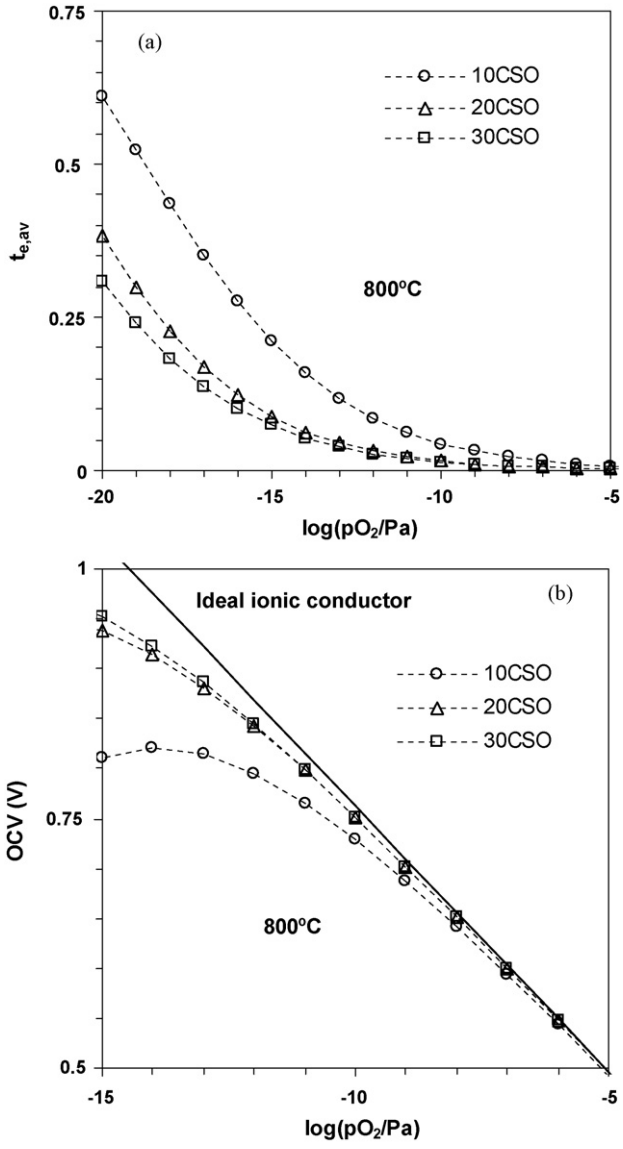

Fig. 14. (a) Average electronic transport number as a function of the oxygen partial pressure in the fuel side when the electrolyte is under an oxygen partial pressure gradient: air/sample/pO_2 and (b) open circuit voltage for the mixed conducting electrolytes as a function of the oxygen partial presure in the fuel side. Straight line represents the open circuit voltage for an ideal ionic conductor obtained by the Nersnt equation.

electrolyte (OCV_{mixed}) is given by the following equation:

$$OCV_{mixed} = OCV_{ion}(1 - t_{e,av}) \quad (5)$$

where OCV_{ion} is the open circuit voltage for an ideal ionic conductor and it is given by the Nersnt equation, and $t_{e,av}$ is the electronic transport number of the electrolyte averaged to the SOFC conditions, that is when the surfaces of the electrolyte are under air and fuel conditions, respectively:

$$t_{e,av} = \frac{\sigma_{e,av}}{\sigma_{e,av} + \sigma_i} \quad (6)$$

where $\sigma_{e,av}$ is the electronic conductivity averaged to the fuel and the air sides of the cell, and σ_i is the ionic conductivity of the electrolyte, assumed constant along the SOFC conditions.

Eq. (5) indicates that changes in the mixed transport properties of the electrolytes affect the obtained value of open circuit voltage, affecting the efficiency of the system.

Ion-blocking measurements were used to obtain independent results of the electronic conductivity of the electrolyte, when the sample is under a gradient of oxygen partial pressure. These results where combined with the ionic conductivity from impedance spectroscopy in air, and we have extracted the corresponding values of $t_{e,av}$ under the assumption of no important dependence of the ionic conductivity on the oxygen partial pressure. Fig. 14(a) shows the average electronic transport number at 800 °C as a function of the oxygen partial pressure in the fuel side (pO_2) for 10CSO, 20CSO and 30CSO electrolytes submitted to a gradient of oxygen partial pressure of air/sample/pO_2. The plot shows a significant increase in the electronic contribution under reducing conditions, mainly in sample with low Sm-content, that is 10CSO. The increase in the n-type electronic conductivity under reducing conditions for samples with lower content of trivalent dopant was previously reported for Gd-doped ceria [27] and it was attributed to the higher reducibility of Ce^{4+}/Ce^{3+} when the Gd-content was decreased. This spoils the efficiency of the fuel cell due to the decrease in the open circuit voltage as it is observed in Fig. 14(b). On the other hand the decrease in the working temperature increases the open circuit voltage, given that the electronic transport number decreases, however the internal resistances of the cell increase considerably. The addition of cobalt to the electrolyte powders produce changes in the mixed transport properties, affecting the open circuit voltage under reducing conditions. Fig. 15 shows the open circuit voltage at 800 °C using H_2 with 10%H_2O as fuel, for electrolyte-samples doped with 2 mol%Co and for Co-free samples. It is appreciable that the OCV is not strongly affected by the addition of Co to the electrolyte, given that the electronic transport number is only slightly changed. Note that the ion-blocking technique could produce some experimental errors in the determination of the electronic conductivity for very reducing conditions. However, the concordance between Co-doped and Co-free samples supports the final results.

The performance of the different systems when they are used in a SOFC configuration was analyzed by the maximum power density that the systems could produce. Theoretical maximum power density is only dependent on the OCV for the used electrolyte and the internal resistances of the cell, that is

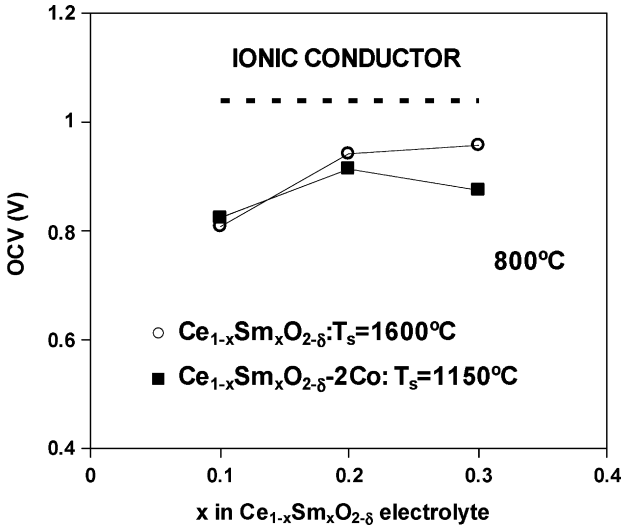

Fig. 15. Open cicuit voltage at 800 °C using H_2 with 10%H_2O as fuel, for $Ce_{1-x}Sm_xO_{2-\delta}$ with (closed squares) and without (open circles) 2 mol%Co-addition as sintering additive. It is also represented the open circuit voltage for an ideal ionic conductor (dashed line).

ohmic resistances (mainly in the electrolyte component), cathode polarization resistance and anode polarization resistance (Eq. (4)). Fig. 16 shows the theoretical maximum power density of the $La_2NiO_4/Ce_{1-x}Sm_xO_{2-\delta}$/anode systems obtained by the ionic–electronic electrolyte conductivities, by the area-specific cathode polarization and anode polarization resistances, using Ni-20CSO as anode with 20CGO electrolyte extracted from results of Ref. [28]. Note that in the obtainment of the power density we have assumed similar values of anode polarization to account differences in cathode performance, and some differences in power density could be obtained by small differences in the assumed values of anode polarization. The electrolyte-

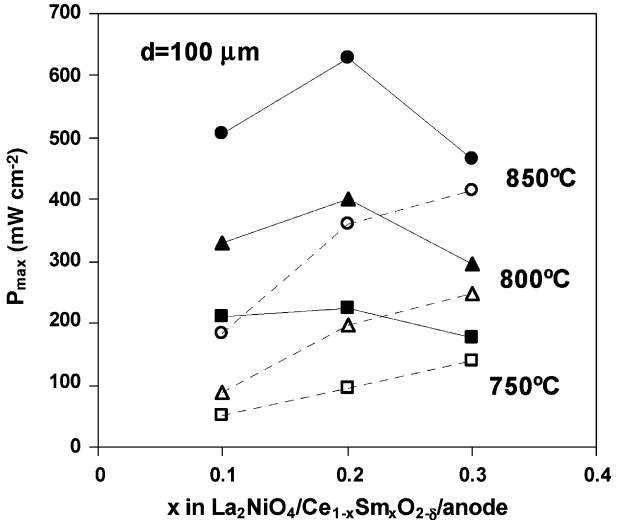

Fig. 16. Theoretical maximun power density as a function of Sm-content in 100 µm thickness $Ce_{1-x}Sm_xO_{2-\delta}$ electrolyte working with La_2NiO_4 as cathode and Ni-20CSO as anode, with anode polarization resistances extracted from Ref. [28]. Open symbols represent electrolytes without cobalt addition sintered at 1600 °C and closed symbols represent electrolytes doped with 2 mol%Co and sintered at 1150 °C.

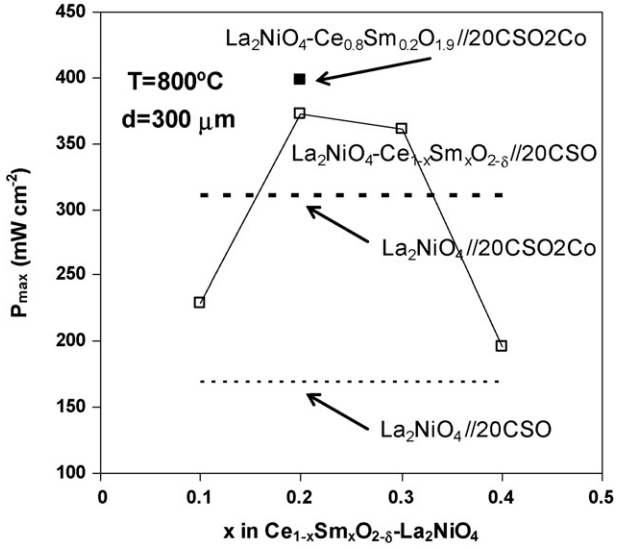

Fig. 17. Theoretical maximun power density as a function of the Sm-content in La_2NiO_4–$Ce_{1-x}Sm_xO_{2-\delta}$ cathode-composites and Ni-20CSO as anode [28], placed on 20CSO and 20CSO2Co electrolytes sintered at 1600 and 1150 °C, respectively, with 300 μm in thickness (squares). For comparison it is also represented the power density of the cells formed by the pure La_2NiO_4 cathode and Ni-20CSO anode on 20CSO2Co (T_s = 1150 °C) and 20CSO (1600 °C) electrolytes (dashed lines).

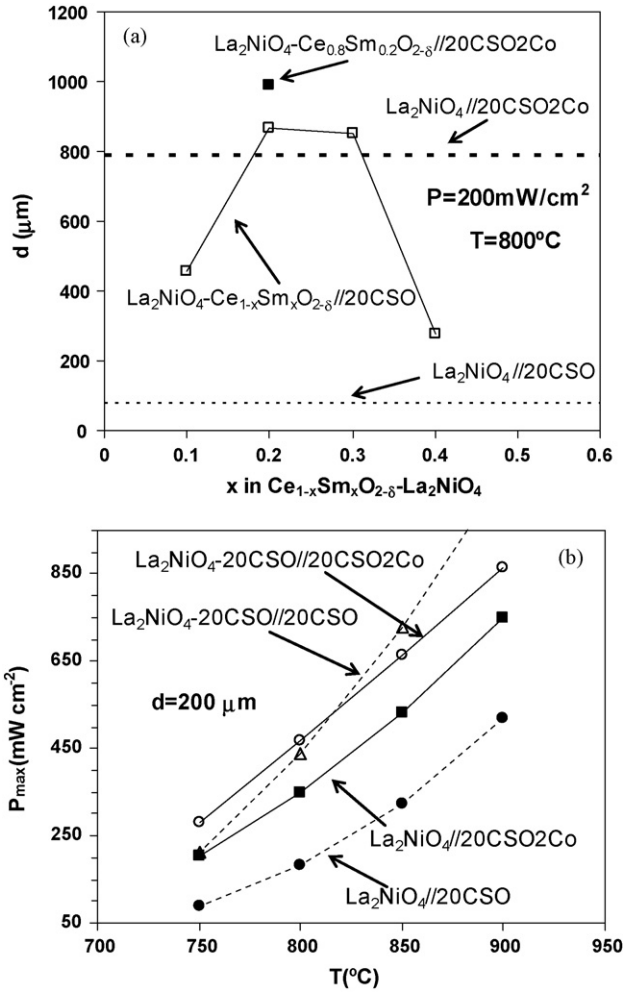

Fig. 18. (a) Maximun electrolyte thickness to obtain a power density of 200 mW cm^{-2} at 800 °C for different La_2NiO_4–$Ce_{1-x}Sm_xO_{2-\delta}$ cathode-composites and Ni-CSO as anode [28] placed on 20CSO (open squares) and 20CSO2Co (closed squares) electrolytes. Electrolyte thickness for pure La_2NiO_4 cathode with 20CSO and 20CSO2Co was also represented. (b) Maximun power density of the cells as a function of operating temperature for electrolyte thickness of 200 μm.

membrane thickness was assumed to be 100 μm. For electrolytes without cobalt addition the performance increases with the increase in Sm-content, due to the lower values of cathode polarization and the higher OCV. At 800 °C is observed an enhancement from 87 mW cm^{-2} for 10CSO electrolyte to 196 and 250 mW cm^{-2}, for 20CSO and 30CSO, respectively. On the other hand, the addition of cobalt and sintering at 1150 °C increases considerably the performance of the cell, mainly due to the important decrease in electrolyte and cathode polarization resistances. The use of these electrolytes could produce performances in the range of 300–400 mW cm^{-2}.

The use of composites as cathode materials is an important feature to improve the efficiency of the cell given the clear decrease in electrode polarization (Figs. 11 and 13). However, the Sm-content in La_2NiO_4–$Ce_{1-x}Sm_xO_{2-\delta}$ composites placed over 20CSO electrolyte clearly affected the polarization resistance (Fig. 12). Fig. 17 shows the theoretical maximum power density at 800 °C as a function of Sm-content in the composites for the cells La_2NiO_4–$Ce_{1-x}Sm_xO_{2-\delta}$/20CSO/anode, La_2NiO_4–20CSO/20CSO2Co/anode, La_2NiO_4/20CSO/anode and La_2NiO_4/20CSO2Co/anode with a typical Ni-20CSO anode material [28] and an electrolyte thickness of 300 μm. The performance of 20CSO electrolyte was previously observed to be highly improved with the addition of 2 mol%Co and sintering at low temperature with the La_2NiO_4 cathode material (Fig. 16). Now the performance is also improved with the use of composites on the 20CSO electrolyte (Fig. 17), and the effect is more accentuated for La_2NiO_4–20CSO and La_2NiO_4–30CSO cathodes, due to their lower polarization resistances when working with 20CSO electrolyte (Fig. 12). On the other hand, the use of 20CSO2Co as electrolyte does not considerably increase the performance when the cathode is formed by the composite La_2NiO_4–20CSO given that the cathode polarization is practically non-affected (Fig. 13).

The enormous decrease in the cathode polarization with the use of composites has important consequences, as the possibility to increase the electrolyte thickness which improves the mechanical stability of the cell. The high electrode polarization of pure La_2NiO_4 with 20CSO electrolyte sintered at 1600 °C forces to decrease the electrolyte resistance to obtain a considerable value of power density. For this reason it makes necessary to decrease the electrolyte thickness. Fig. 18(a) shows the maximum electrolyte thickness for composites and for pure La_2NiO_4 to obtain a maximum power density of 200 mW cm^{-2} at 800 °C. This value was deduced from Eq. (4) by the knowledge of the ionic conductivity and the open circuit voltage of the electrolyte, and the cathode and the anode polarization. As it is observed, the use of La_2NiO_4–20CSO and La_2NiO_4–30CSO composites could allow to increase the 20CSO-electrolyte thickness in a factor of 8–10 compared to

pure La_2NiO_4 cathode. Additionally, if one assumes a value of maximum power density of 250 mW cm^{-2} and an electrolyte thickness of 200 μm, the operating temperature could be decreased from around 825 °C for the La_2NiO_4//20CSO system to around 760 °C for the La_2NiO_4–20CSO//20CSO system (Fig. 18(b)). It is also noticeable that the addition of 2 mol%Co to the 20CSO electrolyte has no important effect on the efficiency of the system at temperatures below 825 °C when the cathode material is based on the composite La_2NiO_4–20CSO. However, the use of this electrolyte clearly increases the efficiency of the system when the cathode material is based on pure La_2NiO_4.

4. Conclusions

$Ce_{1-x}Sm_xO_{2-\delta}$ electrolyte-system ($x = 0.1$, 0.2, 0.3, 0.4) was employed to analyze the electrode polarization with La_2NiO_4 cathode material. The electrode performance was clearly affected by changes in the electrolyte properties, showing an important enhancement in the interface polarization with the increase in the Sm-content. Electrolytes were doped with 2 mol%Co to decrease the sintering temperature and the ionic resistance, and this also resulted in an important decrease in the electrode polarization. Electrolyte grain boundary properties were in concordance with the interface properties suggesting that the oxygen ion transference from the interface into the electrolyte dominates the electrode performance in the studied materials. The use of composites as cathodes enhanced considerably the electrode polarization due to the increase of the ionic conductivity and the corresponding enlargement of the surface reaction in the cathode. The electrolyte ionic–electronic transport properties under a pO_2 gradient and the cathode polarization in air, combined with the typical anode polarization in H_2 allowed to obtain an estimation of the power density of the cell in SOFC conditions. The optimization of the properties of both the cathode and the electrolyte allowed to increase the performance in more than a factor of two. Estimated values of power density of 400 mW cm^{-2} at 800 °C were obtained for a 20CSO2Co electrolyte with 300 μm in thickness, working with the cathode composite La_2NiO_4–20CSO.

Acknowledgements

This work was supported by the Community of Madrid (Project ENERCAM-CM; S-0505/ENE/0304) and by the Spanish Education and Science Ministry (Project MATSOFC; MAT2005-02933). One of the authors (D.P.-C.) wishes to thank the Spanish Education and Science Ministry for financial support ("Programa Juan de la Cierva").

References

[1] B.C.H. Steele, K.M. Hori, S. Uchino, Solid State Ionics 135 (2000) 445.
[2] B.C.H. S Steele, Proceeding of the First European SOFC Forum, vol. 1, U. Bossel, Lucerne, 1994, p. 375.
[3] H.J.M. Bouwmeester, A.J. Burgraaf, in: A.J. Burgraaf, L. Cot (Eds.), Fundamentals of Inorganic Membrane Science and Technology, Elsevier, Amsterdam, 1996, p. 435.
[4] V.V. Kharton, A.P. Viskup, A.V. Kovalevsky, E.N. Naumovich, F.M.B. Marques, Solid State Ionics 143 (2001) 337.
[5] J.A. Kilner, C.K.M. Shaw, Solid State Ionics 154–155 (2002) 523.
[6] A. Aguadero, J.A. Alonso, M.J. Martínez-Lope, M.T. Fernández-Díaz, M.J. Escudero, L. Daza, J. Mater. Chem. 16 (2006) 3402.
[7] E. Boehm, J.-M. Bassat, P. Dordor, F. Mauvy, J.-C. Grenier, P. Stevens, Solid State Ionics 176 (2005) 2717.
[8] D. Pérez-Coll, P. Núñez, J.R. Frade, J. Electrochem. Soc. 153 (3) (2006) A478.
[9] D. Pérez-Coll, P. Núñez, J.R. Frade, J.C.C. Abrantes, Electrochim. Acta 48 (2003) 1551.
[10] J.C.C. Abrantes, D. Pérez-Coll, P. Núñez, J.R. Frade, Electrochim. Acta 48 (2003) 2761.
[11] C. Kleinlogel, L.J. Gauckler, Solid State Ionics 135 (2000) 567.
[12] D.P. Fagg, J.C.C. Abrantes, D. Pérez-Coll, P. Núñez, V.V. Kharton, J.R. Frade, Electrochim. Acta 48 (2003) 1023.
[13] M.H. Hebb, J. Chem. Phys. 20 (1952) 185.
[14] C. Wagner, Proceedings of the Seventh Meeting of the International Committee on Electrochemical Thermodynamics and Kinetics, Lindau, Butterworths Scientific Publication, London, 1957, p. 361.
[15] L. Navarro, F. Marques, J.R. Frade, J. Electrochem. Soc 144 (1) (1997) 267.
[16] S. Lübke, H.D. Wiemhofer, Solid State Ionics 117 (1999) 229.
[17] D. Pérez-Coll, D. Marrero-López, P. Núñez, J.C.C. Abrantes, J.R. Frade, J. Solid State Electrochem. 8 (9) (2004) 644.
[18] D. Pérez-Coll, P. Núñez, J.C. Ruiz-Morales, J. Peña-Martínez, J.R. Frade, Electrochim. Acta 52 (2007) 2001.
[19] C. Fu, K. Sun, N. Zhang, X. Chen, D. Zhou, Electrochim. Acta 52 (2007) 4589.
[20] M.J. Escudero, A. Aguadero, J.A. Alonso, L. Daza, J. Electroanal. Chem. 611 (2007) 107.
[21] E.P. Murray, S.A. Barnett, Solid State Ionics 143 (2001) 265.
[22] X. Xu, Z. Jiang, X. Fan, C. Xia, Solid State Ionics 177 (2006) 2113.
[23] E.P. Murray, T. Tsai, S.A. Barnett, Solid State Ionics 110 (1998) 235.
[24] D. Pérez-Coll, J. C. Ruiz-Morales, D. Marrero-López, P. Núñez, J.R. Frade, J. Alloy. Compd., in press, doi:10.1016/j.jallcom.2007.12.039.
[25] V.V. Kharton, A.P. Viskup, F.M. Figueiredo, E.N. Naumovich, A.L. Shaulo, F.M.B. Marques, Mater. Lett. 53 (2002) 160.
[26] D. Pérez-Coll, D. Marrero-López, P. Núñez, S. Piñol, J.R. Frade, Electrochim. Acta 51 (2006) 6463.
[27] D. Pérez-Coll, D. Marrero-López, J.C. Ruiz Morales, P. Núñez, J.C.C. Abrantes, J.R. Frade, J. Power Sources 173 (2007) 271.
[28] S. Wang, T. Kato, S. Nagata, T. Kaneko, N. Iwashita, T. Honda, M. Dokiya, Solid State Ionics 152–153 (2002) 477.